The liquid wave characteristics during the transportation of air-water stratified co-current two-phase flow in a horizontal pipe

Akhmad Zidni Hudaya[a,b], Arif Widyatama[a,c], Okto Dinaryanto[d], Wibawa Endra Juwana[a,e], Indarto[a,c], Deendarlianto[a,c,*]

[a] Department of Mechanical and Industrial Engineering, Faculty of Engineering, Universitas Gadjah Mada, Jalan, Grafika 2, Yogyakarta 55281, Indonesia
[b] Department of Mechanical Engineering, Universitas Muria Kudus, Kampus Gonandgmanis, Kudus, Central Java, Indonesia
[c] Center for Energy Studies, Gadjah Mada University, Sekip K-1A Kampus UGM, Yogyakarta 55281, Indonesia
[d] Department of Mechanical Engineering, Sekolah Tinggi Teknologi Adisutjipto, Blok R Lanud Adisutjipto, Yogyakarta 55198, Indonesia
[e] Department of Mechanical Engineering, Faculty of Engineering, Universitas Sebelas Maret, Jalan, Ir. Sutami 36A, Surakarta, Indonesia

A B S T R A C T

The understanding of the interfacial wave structure and its effect to the interfacial friction factor is important to reveal the transition from stratified to the slug flows. However, the available theoretical of models, as well as the correlations to predict the wave interfacial characteristics, is quite rare. The discrepancy among researchers is often found. In the present work, the wave characteristics of air-water stratified flow were investigated experimentally. The inner diameter was 26 mm. The liquid superficial velocity (J_L) raised from between 0.02 m/s and 0.075 m/s while the gas superficial velocity (J_G) ranged from 4 m/s to 16 m/s. A high speed camera was used to capture high-quality visual data which was later processed with the image processing technique.

As a result, the quantitative parameters of the stratified flow were successfully determined and analyzed. Next, the dimensional analysis was carried out to develop correlation to predict the flow parameters of the wave such as the wave frequency, the wave velocity, the wave amplitude, and the wavelength. Furthermore, it is found that the ratio of gas and liquid Reynolds number and Martinelli Parameter plays important role in almost all of the proposed correlation.

1. Introduction

The gas-liquid stratified and wavy flow can be easily found in various industrial processes such as the transportation system in oil and gas industry, nuclear reactor cooling system, and a geothermal plant. The interfacial wave generated by the slip ratio between the gas and liquid superficial velocity strongly affects the characteristic of the flow. That phenomenon indicates that the presence of interfacial wave has a significant effect on the pressure drop [1]. In addition, the interfacial wave also leads the increase of the mass and heat transfer rates both at the interface and at the pipe walls [2].

The complex phenomena of the interfacial wave cause researchers to elaborate the recent studies and expand the investigation into numerous novel topics. For instance, it is generally noted that the wave characteristics plays important role on the regime transition of two phase flow. In detail, the interfacial characteristics of the stratified flow is considered as the main parameter to predict the transition mechanism to the slug flow [3–6]. While the wave growth and evolution are strongly decisive in the viewpoint of atomization and the droplet deposition which leads the transition condition of annular flow [7]. Furthermore, Woodmansee and Hanratty [8] reported that the detailed

information of the wave characteristics should be defined carefully in order to develop a theoretical model accurately.

To create a reliable transportation system that able to maintain the presence of the stratified flow, it is very important to understand the stratified flow itself [9]. In these three decades, researchers have drawn their attention to study the characteristics of the stratified flow, and it was found that various different interfacial wave exists during the stratified flow [10–12]. Speeding and Nguyen [10] performed the visualization study of the stratified flow in horizontal pipes. The results revealed that the stratified flow was divided into four main sub-regimes. Those are: stratified (smooth), stratified + ripple wave, stratified + roll wave, and stratified + inertial wave. However, Chen et al. [11] realized that under a high gas superficial velocity, the detailed of the wave behavior was very difficult to be observed. Other experimental works have been carried out by also Fernandino and Ytrehus [12] and Tzotzi and Andritsos [2]. They classified the stratified flow into five regimes: stratified smooth, regular wave (2D and 3D wave), irregular large-amplitude wave or roll wave, and droplet atomization. Furthermore, a new flow pattern, which is identified as pseudo-slug flow, was introduced by Lin and Hanratty [7]. Whereas the main characteristic of this flow pattern is defined as the presence of the

---

temporary blockage during the flow.

Numerous experimental techniques and analysis methods have been developed to achieve a depth understanding of the wave characteristics, such as conductance probe [13–15], capacitance probe [16,17], Particle Image Velocimetry [18,19] and image processing [20–22]. The conductance probe is often used for the conductive working fluid such as water and the water solution. On the other hand, for nonconductive fluids (oil and natural gas), the capacitance probe can be considered as a suitable measurement method to determine the wave interfacial behavior [16,17].

Recently, image processing becomes one of the most frequent methods to analyze the two phase flow behavior. Furthermore, this technique offers also numerous benefits like the non-intrusive characteristics, easy to calibrate, and the flexibility to be implemented on various flow pattern. Equally important, the fast development of the optical tools and the personal computer also influence the application of this method. The image processing technique has been utilized to gather the information of interfacial characteristics of two-phase flow by previous researchers such as Morales et al. [23], do Amaral et al. [24], and Widyatama et al. [25]. On the other side, this technique still offers a great opportunity for improvement in term of optimizing the available algorithm to obtain a high quality quantitative data and achieve a shorter time processing.

In term of determining the dynamics property of wave characteristics in two phase model, previous studies have provided a specific approached which can be used in the further investigation [1,26–28]. For example, the dominant frequency is usually determined by power spectrum method [1,26–28]. The application of the fast Fourier transform (FFT) to analyze the domain frequency of the time variation data of the film thickness is also considered. Some of the researchers combined the above method with the visual observation [29,17,6]. Another important parameter that should be investigated is wave velocity which is usually measured by the cross-correlation method [15,17,1,28]. Here, two sets of wave signal data are calculated simultaneously to obtain the lag time between the data. While the radial wire mesh sensor has been utilized by Kong et al. [30] to measure the axial velocity distribution. Regarding the wave amplitude Andritsos [31], Paras and Karabelas [26], and Gawas et al. [17] have formulated the amplitude of the wave as a linear function of the deviation standard of the film thickness data. On the other hand, researchers such as Mantilla [29], Castro and Rodriguez [21], Kuntoro et al. [22] and Bae at al. [28] calculated the amplitude of the wave by subtracting the average of wave peak with the wave valley. Next, they defined the wavelength as the difference between two consecutive wave peak and it can be obtained by multiplying the wave velocity and the moving time of the wave. In addition, the wavelength is also determined by dividing the wave velocity with the wave frequency. In summary, the different method that has been used to gather the wave interfacial characteristics often causes the difference in both of results. In addition, the experimental condition and the theoretical assumption of the model also plays a significant role in the discrepancy of the produced data. Therefore, further experimental studies in order to enhance the available database and clarify the previous results should be conducted.

Table 1 shows the summary of previous studies including the experimental correlation related to the wave properties. From the table, it is noticed that the presence of the experimental correlation of the dynamic properties of the stratified flow is quite rare. In addition, the discrepancy among the available correlation as well as the factor strongly affected the wave characteristics is clearly found.

The aim of the present experimental work is to investigate the characteristics of the interfacial wave of the stratified flow. Here, the image processing technique was chosen as the main method to obtain the quantitative parameter of the stratified flow data. The data was comprehensively analyzed and compared to the result from the previous studies. In addition, the dimensional analysis was also performed to reveal any factor affecting the wave characteristics of the slug flow.

The quantitative data obtained from the present work is important to fulfill the need for a high-quality database of stratified flow as well as to justify the available model. Equally important, the detailed information of the wave characteristics can be used to develop a transition model of stratified flow to slug flow and support the validation of the available CFD codes [32].

2. Experimental apparatus and procedure

The experiments were performed at the Laboratory of the Fluid Mechanics, Mechanical and Industrial Engineering Departement, Universitas Gadjah Mada. The installed research facility is shown in Fig. 1 which consist of the horizontal pipe, compressor, water supply pump, flowmeter, mixer, and separator. In the present work, a set of 26 mm inner diameter was arranged with a total length of 10 m. A simple T mixer, as shown in Fig. 2, was installed on the inlet section where the air was injected from upper part while the water was supplied from the bottom part. In the middle of the mixer, 3 mm spliter plate was placed to reduce the flow fluctuation.

A compressor at the maximum amount of 600 LPM and pressure of 8 bars (gauge) was used to obtain the desired airflow rate. Here, the air regulator was also utilized to control a constant inlet pressure. In order to control the air flow rate, three Dwyer gas rotameters with maximum capacities of 200, 600 and 1600 SCFH, and approximately 3% accuracy were used. The water supply was fulfilled by pumping the water from the storage tanks. A centrifugal pump with a maximum capacity of 16.8 m³/h, was used. To measure the water flow rates, the Omega water rotameter with a maximum capacity of 75 GPH and approximately 2% accuracy was used. In addition, to minimize the flow oscillations and vibrations at around inlet area, a flexible hose was installed. Next, the air and the water flowed co-currently in the test section. At the end of the test section, a separator was installed. Here, the air was released into atmosphere and the water was collected on the storage tanks before it was pumped back to the inlet section.

The experiments were performed under the atmosphere condition. It was assumed that the system was not affected by surroundings, hence there was no heat transfer process passing the system boundary. The water superficial velocity (J_L) ranged from 0.02 m/s to 0.075 m/s and the air superficial velocity (J_G) was set between 4 m/s and 16 m/s.

To ensure the fully developed stratified flow, the observation area was set on the 180 D from the inlet. The scheme of observation area is depicted in Fig. 3(a). Here, a correction box was placed to minimize the refraction effect of the acrylic pipe. In order to support the flow visualization, a set of LED lamps and a diffusive layer was arranged behind the pipe. A high speed video camera Phantom Miro M310 was used which produces 3200 fps on the maximum image resolution, 1280 × 800. The focal length and the aperture of the lens were 85 mm and 2.8, respectively. Hence, a 2 mm depth-of-field was obtained. As illustrated in Fig. 3(b) the out of area produces blurry interface so the observation can be only focused in the centre of the pipe. In the present study, the high speed video camera was set between 200 and 800 fps to capture the detailed phenomena of the stratified flow.

Before the phenomena of the stratified flow were captured, there were two steps that should be conducted. First, a calibration object was placed in the middle of the correction box. This step was essential to achieve an accurate focus point of observation. Next, it was also important to capture the image of full water and the full air which will be used in the background subtraction later.

2.1. Image processing technique

In the present experimental work, the interfacial wave characteristics were obtained by using image processing technique. Fig. 4 presents the sequential steps of the image processing technique. Six main steps were introduced before the analysis of quantitative parameter was conducted. First, the sequence images were loaded to the Matlab

Table 1
The summary of the previous research on the wave characteristics and the proposed correlation.

| Author	Working Fluids	Geometry	J_G and J_L (m/s)	Regime	Wave Equation
Ousaka et al. [34]	Air–water	Pipe dia. = 25.4 mm	16–30 0.04–0.1	Annular	Freq. $f = 0.0066 \frac{J_L}{D} \left(\frac{Re_G}{Re_L} \right)^{1.18}$ Velocity, $c = 3.0 J_L \left(\frac{Re_G}{Re_L} \right)^{0.78}$
Paras et al. [26]	Air–water	Pipe dia. = 50.8 mm	10–66 0.02–0.2	stratified - Annular	Velocity , $c = 0.75 + 0.002 \left[J_G^5 \left(\frac{h_L}{D} \right) \right]^{0.5}$
Mantilla [29]	Air–water	Pipe dia. = 50 and 152 mm	5–80 0.0035–0.01	Stratified - Annular	Freq. St = $0.25 \, X^{-1.2}$ Velocity, $c = \frac{\psi U_G + U_L}{1 + \psi}$; Amplitude, $\frac{\Delta h_w}{h_L} = 1350 \frac{Re_G^{0.1}}{Re_L^{0.5}} - 3.25$ for $\frac{Re_G^{0.1}}{Re_L^{0.5}} \leq 0.005$
Al Sarkhi et al. [15]	Air–water	Pipe dia. = 0.076 mm	40–80 0.0035–0.004	Annular	Freq. St = $1.1 \, X^{0.93}$ Velocity, $c/j_L = 2.379 \, X^{-0.9}$
Gawas et al. [17]	Air–oil	Pipe dia. = 152.4 mm	10–20 0.005–0.02	Stratified - Annular	Freq. St = $5.102 \, X^{-0.495}$ Velocity, $c/j_L = 3.51 \, X^{-0.81}$ Amplitude, $\frac{\Delta h_w}{D} = 0.67 \left(\frac{\Delta h_w}{D} \right)^{0.71}$ $\frac{\Delta h_w}{D} = 0.58 (X)^{0.53}$
Bae et al. [28]	Air–water	Rectangular channel = 40 × 50 mm	5–25 0.01–0.08	Stratified	Freq. St = $0.057 X^{-1.33} + 0.89$ Amplitude, $\frac{\Delta h_w}{h_L} = 3.84 exp \left[- \left[\frac{\frac{Re_G^{0.1}}{Re_L^{0.5}} - 0.0067}{0.0053} \right]^2 \right]$ for $\frac{Re_G^{0.1}}{Re_L^{0.5}} \leq 0.005$
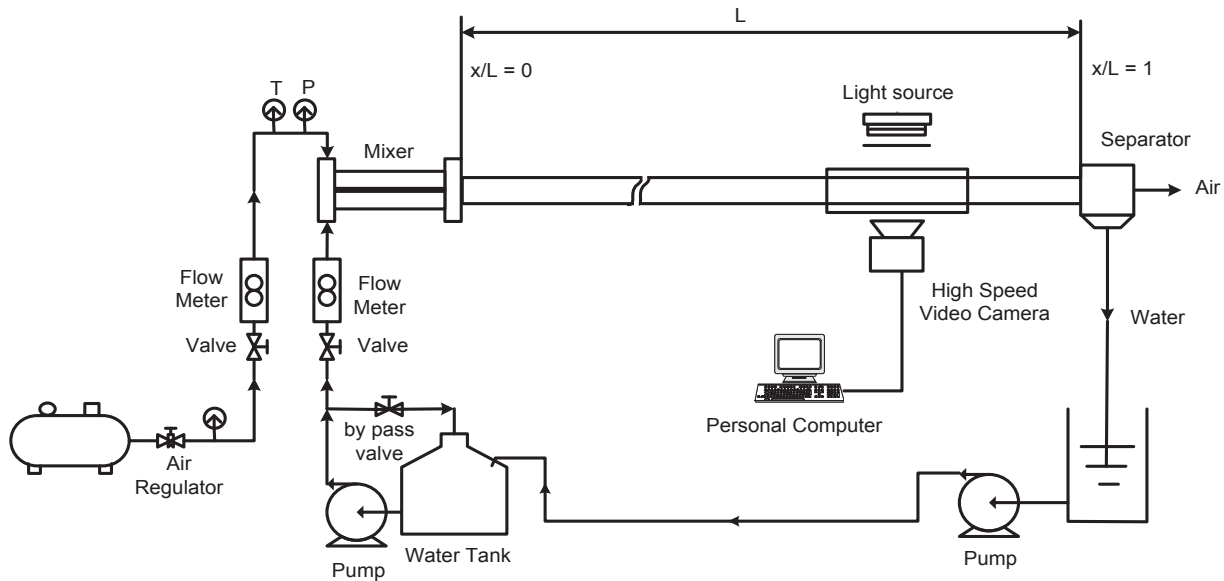
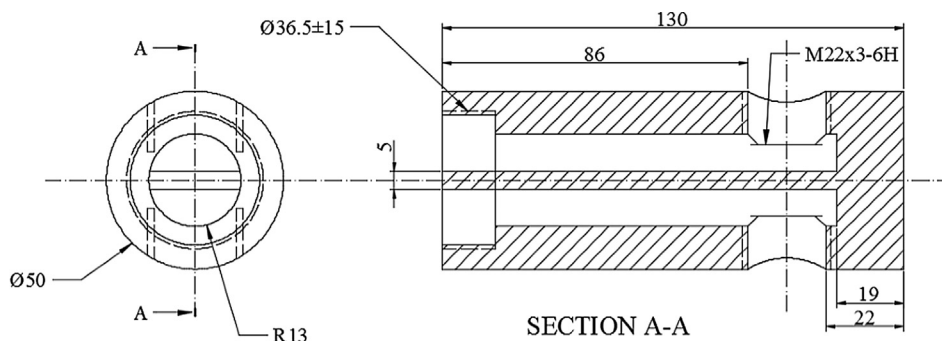**Fig. 1.** The schematic diagram of the experimental apparatus.

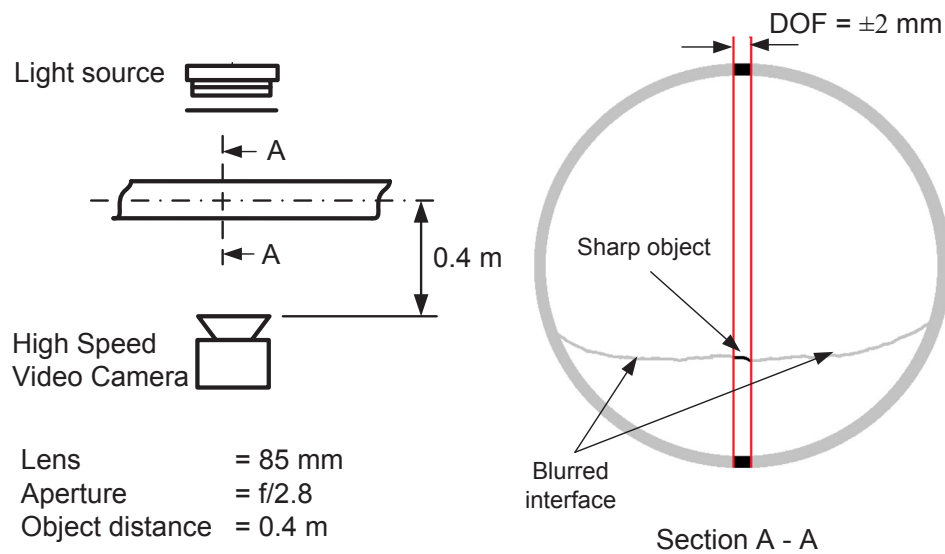**Fig. 2.** The configuration of the simple T mixer.

Fig. 3. (a) The scheme of observation area. (b) The cross sectional view of the horizontal pipe.
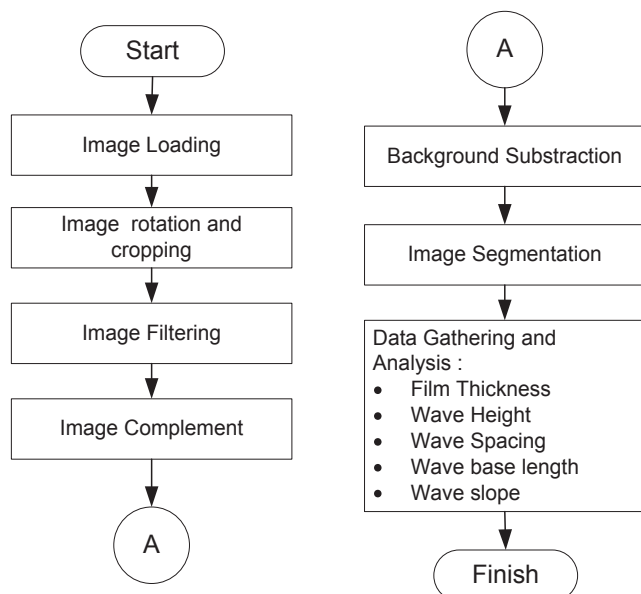

Fig. 4. The image processing steps at longitudinal section.

R2013a. It was set as a raw grayscale image. Before the further steps was executed, the condition of raw image should be checked in order to ensure the position of the object. The rotation process was applied to fix the misalignment between the length of the pipe and the horizontal axis of the image. The cropping process was also implemented to remove unused part of the image. Next, the image filtering was done to enhance the image quality. As suggested by do Amaral et al. [24] and Widyatama et al. [25], the combination of filter bottom hat filter and top hat filter was used to increase the image contrast (Fig. 5(b)).

The next steps reversed the each value of the pixel with its complement value. The result of the complement process is shown in Fig. 5(c) where in comparison to the previous one, the processed image contains the brighter air-liquid interface and darker background image. Then the background subtraction process, as applied by Vallée et al. [33] and Kuntoro et al. [22], was carried out. This steps mainly was used to reduce any uneven condition on the image. The value of liquid film thickness was determined by finding the maximum grayscale value of each column. Next, the distance of the air-liquid interface and the bottom of the image was determined and it represented the film

thickness of the stratified flow. The result of this process is depicted in Fig. 5(f). In detail, the figure shows the raw image which is overlapped by the obtained liquid air interface (red line).

It is realized that the implementation of shadowgraph method produces limitations, such as the presence of local blindness due to the interface blockage which occurs in front of the measuring plane. As a result, the local film thickness sometimes cannot be detected accurately. However, this method still offers numerous advantages and moreover it can be developed through various available algorithm to minimize the problems. Recently, Widyatama et al. [25] have proposed sequence steps to overcome the limitation of slug flow object measurement due to the presence of dispersed bubble. It produces a better object recognition in comparison to the conventional binary conversion procedure. In term of the measurement of film thickness, Kuntoro et al. [22] and Motonya et al. [20] have proposed specific methods to overcome the problem of the inaccurate film thickness detection due to interfacial oscillation. In the present work, median, and top and bottom hat filter were applied. Median filter is used to reduce the noise while the combination top hat filter and bottom hat filter produce an image containing a better contrast composition. On the most of 3D wave pattern case, the filter Savitzky-Golay is used to interpolate the interface contour. The filter was set on polynomial order of 3 as used by Gowri et al [34] (see Fig. 6b). Although those sequence methods has successfully solved the problem on the 3D wave interface, a more advanced process to extract quantitative parameter on this regime should be developed on the further study since in the present study, the data can be biased by the use of the filter especially on the 3D wave pattern with high oscillation frequencies.

Fig. 6 indicates the implemented process to overcome the presence of local blindness during the film thickness measurement. In Fig. 6(a), the front side of the 3D wave shows a blurry interface. It is probably due to the 3D wave pattern which oscillates around the centre of the pipeline. The treatment applied in this case is shown in Fig. 6(b). In the left side, the edge detection process cannot optimally perform due to the blurry interface. Consequently, the results show a fluctuated interface. Whereas the right side of Fig. 6(b) depicts the result of the smoothing process applied in this works. As shown in the figure, the problem due to local blindness can be overcame. In addition, the result of edge detection is plotted in Fig. 6(c), and it shows a well-represented stratified interface.
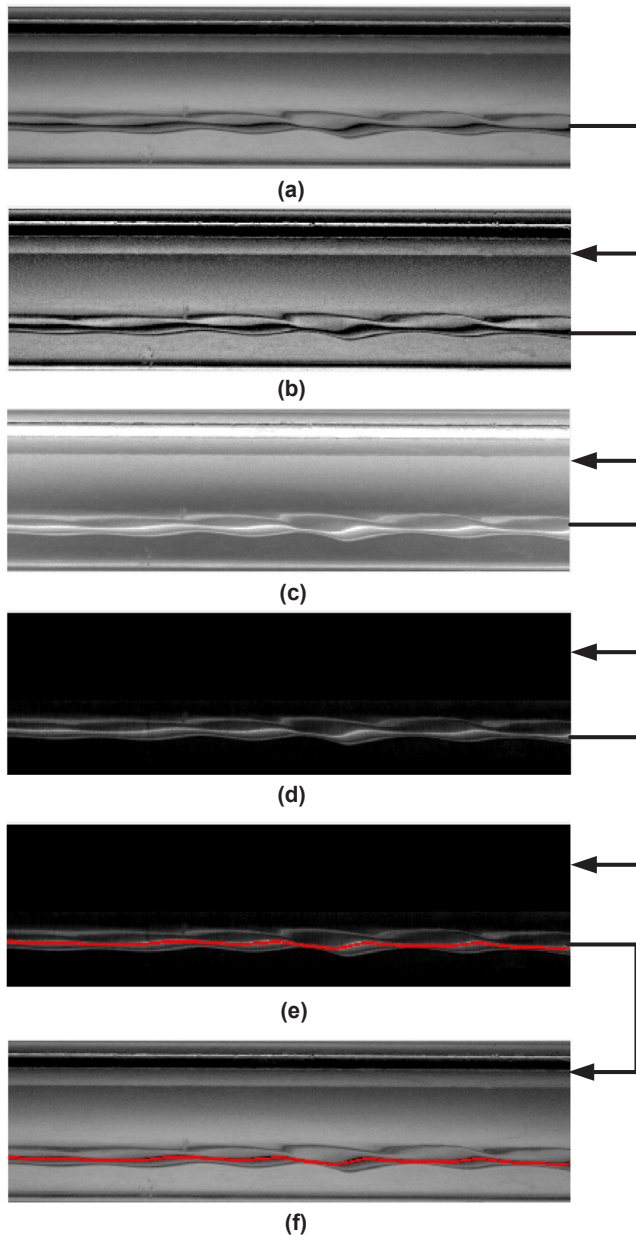
Fig. 5. (a) Raw image. (b) Image after filtering process. (c) Image after complement process. (d) Image after background substraction process. (e) Film thickness detection process. (f) Film thickness detection result is plotted in the grayscale image.

2.2. Wave parameter measurement

The comprehensive understanding of the wave characteristics is important to evaluate two phase flow model. Here, the parameters which will be discussed are the film thickness, the wave amplitude, and the wavelength.

a. Film thickness

Film thickness is the main parameter which is essential to extract the other interfacial characteristics of the stratified flow. The measurements were done in four reference points as shown in Fig. 7. Each reference point produced the film thickness time series data as illustrated in Fig. 7(b).

The example of the film thickness time series information is shown in Table 2. From the table, it is noticed that each flow pattern produces different pattern of the film thickness time series data. For example, the 2D wave is characterized by the presence of small amplitude as well as the uniform period wave acting as sinusoidal wave. The 3D wave is denoted by presence of bigger the wave amplitude. The irregular wave can be found although the uniform wave still dominant in this case. Close observation of Table 2 reveals also that the roll wave and pseudo slug pattern show the intermittent pattern.

b. Wave Frequency

In the present experimental study, the dominant wave frequency was determined by using the fast fourier transform (FFT). The frequency was determined by the value of frequency axis corresponding to the maximum FFT value as shown in Fig. 8. In the figure, under a constant J_L of 0.03 m/s, the $J_G = 5$ m/s and $J_G = 16$ m/s were chosen as the example. In order to validate the obtained dominant frequency from Fast Fourier Transform (FFT), manual counting from the film thickness time trace was conducted.

c. Wave Velocity

As shown in Fig. 7, each reference measurement point produces a film thickness time series data. As a result, a brief comparison of each data can be performed to obtain the wave velocity. Here, the wave velocity, represented by lag time, was determined by using the cross correlation method of two set of time series data. The cross corelation of $R_{xy}(t)$ gathered from $x(t)$ and $y(t)$ is described as follows:

$$R_{xy}(t) = \int_{-\infty}^{\infty} x(\tau)y(t + \tau)d\tau \tag{1}$$

where t is the lag time and R_{xy} is defined as the cross correlation function of the $x(t)$ and $y(t)$

d. Wave Amplitude

Each time series data of air-liquid stratified flow obtained from the image processing technique can be approached as the signal wave flow. One of the wave characteristics is the wave amplitude. The wave amplitude (Δh_w) is defined as the difference between wave height (h_w) and the wave base height (h_{LB}). This method was also introduced by Mantilla [29]. The wave height (h_w) is determined from average of wave peaks above the mean film thickness plus 1.5 of the standard deviation. On the other hand, the wave base height (h_{LB}) is determined from the average of wave valleys below the mean film thickness -0 to -1.5 standard deviation. Fig. 9 presents the example of the characteristics of local film thickness of the wave. Here the flow condition was $J_L = 0.03$ m/s and $J_G = 12$ m/s.

e. Wavelength

The wavelength is defined as the difference between two consecutive wave peak. It was obtained by multiplying the wave velocity and the moving time of the wave. Close observation of Fig. 9 between 8.8 and 10 s illustrates the example of wave unit. The unit wavelength is represented by L_w symbol. In general, the average wavelength is calculated as follows:

$$L_w = \frac{c}{n} \sum_{i=1}^{n} (t_i - t_{i-1}) \tag{2}$$

where c is the wave velocity, n is the number of wave during the experiments, and t_i is the time when wave reaches the peak i.

3. Results and discussion

As the liquid and gas superficial velocities were set on the desired

(a) the raw Image

(b) the film thickness detection result

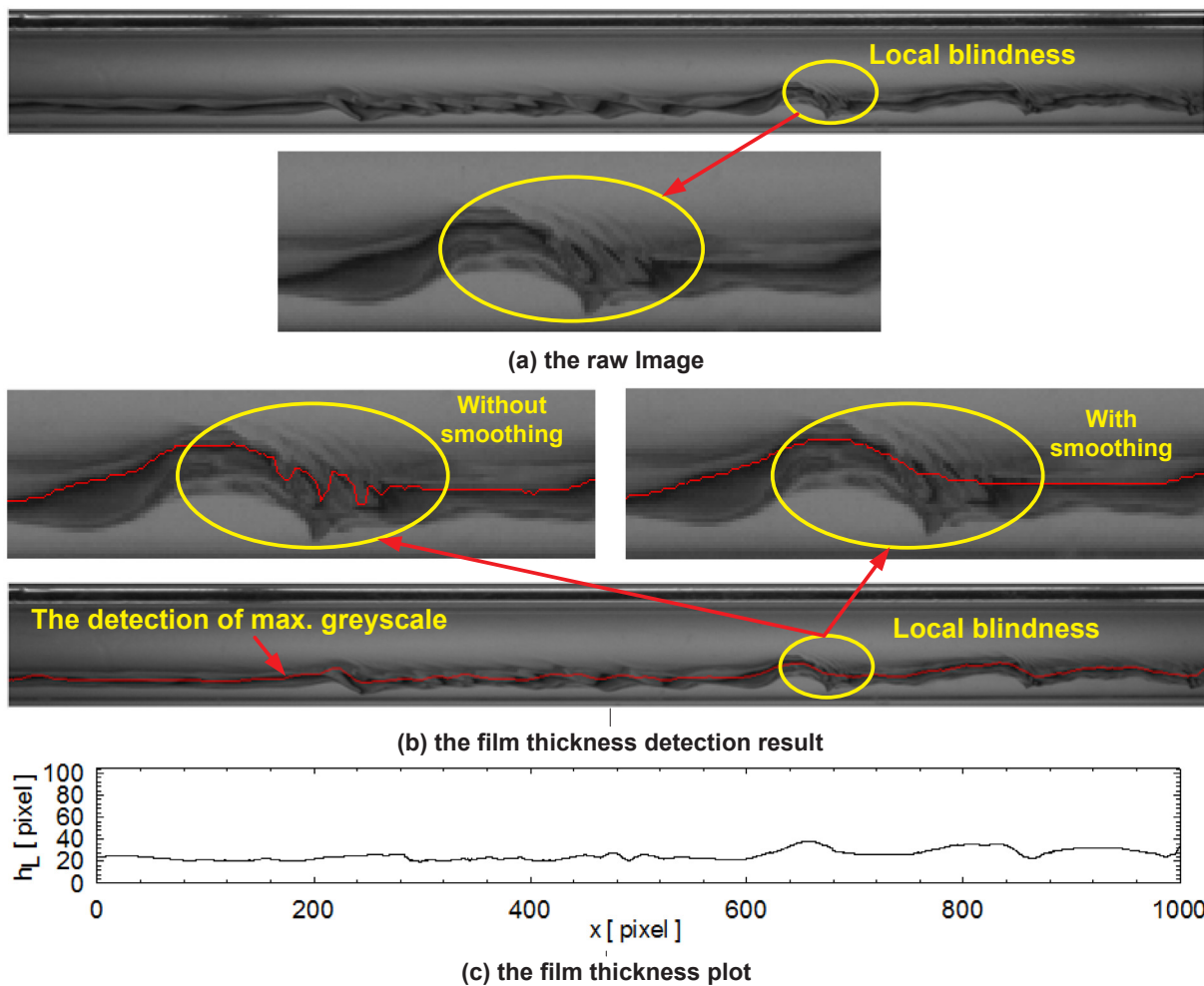**(c) the film thickness plot**

Fig. 6. Smoothing process to detect the local film thickness on the wavy stratified flow.

flow condition, the visualization study utilizing a high-speed video camera was carried out to obtain the brief description on the interfacial wave structure of the stratified flow. Next, the image processing technique was applied to determine the quantitative parameters of the stratified flow in a horizontal pipe such as the film thickness, the wave frequency, and the wave amplitude. In the next following section, the

(a)   (b)
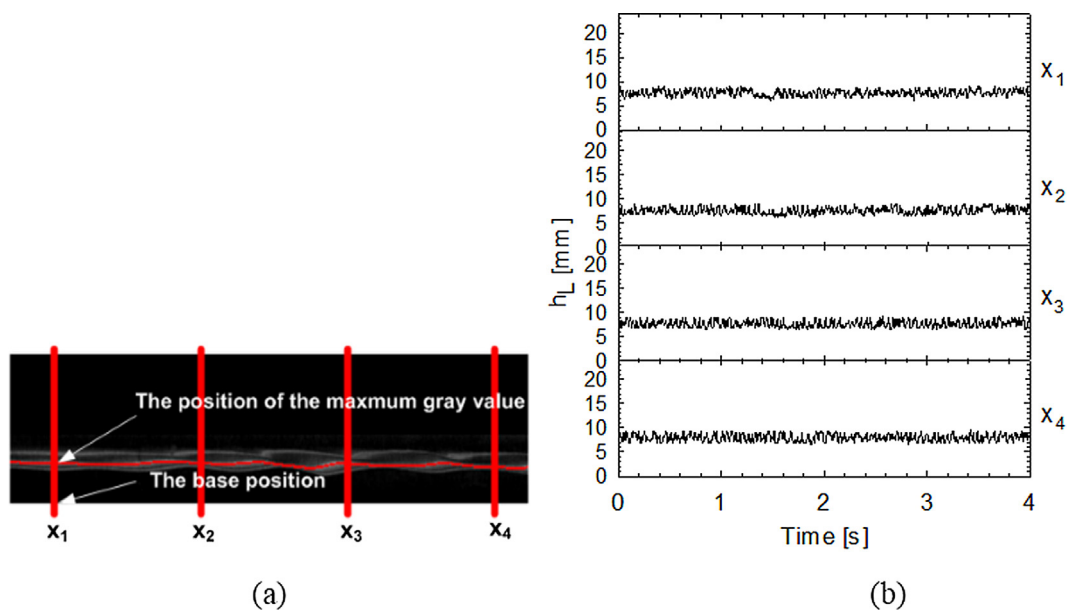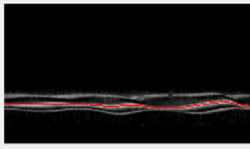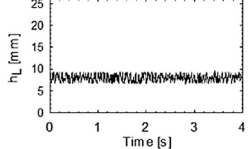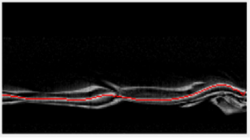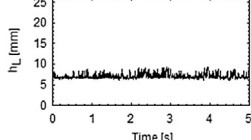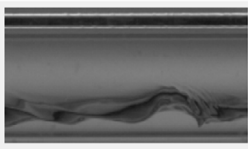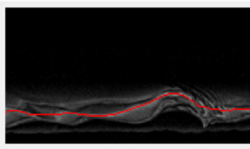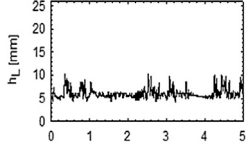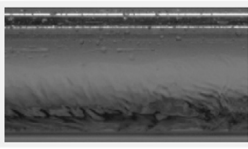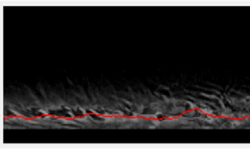
Fig. 7. (a) the film thickness detection result at four different reference positions, (b) the time series plot.

Table 2
The examples of the wave pattern were identified with the image processing analysis.

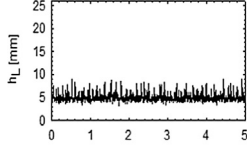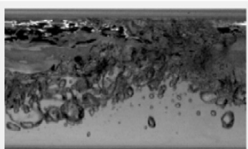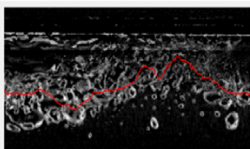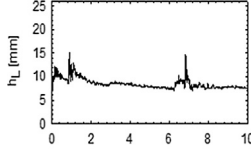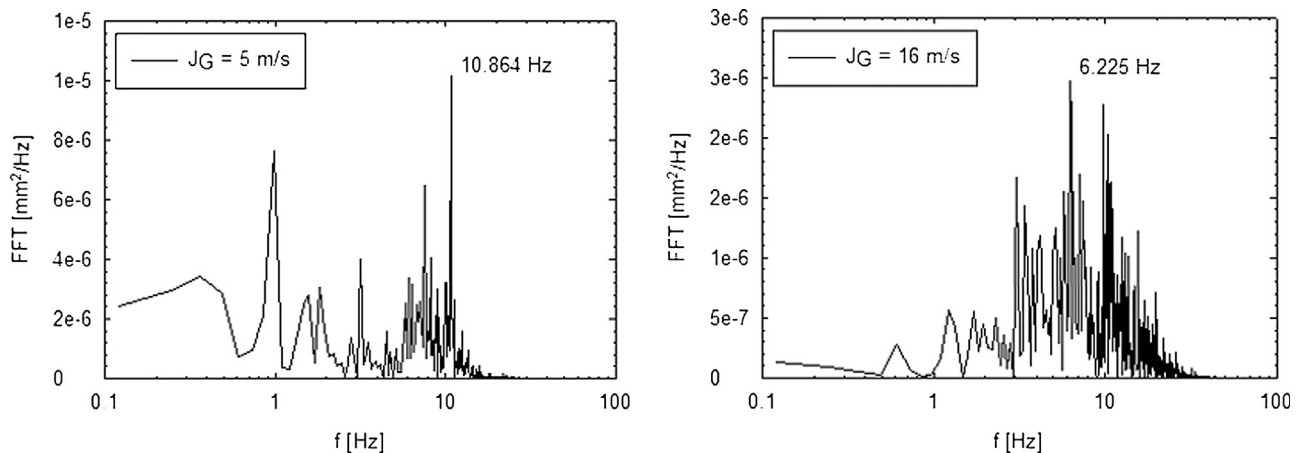| Data	The original image	The processed image	The time series plot
2D Wave JL = 0.03 m/s JG = 5 m/s			
3D Wave JL = 0.03 m/s JG = 6 m/s			
Roll Wave JL = 0.03 m/s JG = 8 m/s			
Entrained Droplet + RW JL = 0.03 m/s JG = 16 m/s			
Pseudo Slug JL = 0.05 m/s JG = 5 m/s			

Fig. 8. The determination of wave frequency with FFT method at constant J_L of 0.03 m/s.

analysis of image visualization is presented first followed by wave regime map on the present work. Next, the wave parameters will be comprehensively discussed. To provide a better understanding of the wave characteristics, the dimensional analysis of each parameter will be performed. As a result, the effect of both liquid and gas superficial velocity as well as any non dimensional number were successfully revealed.

3.1. Interfacial wave pattern

Fig. 10(a) shows the example of 2D wavy flow pattern. Here, the flow condition of the J_L = 0.03 m/s and J_G = 4 m/s was an example. In

this flow pattern, the gas-liquid phase was fully separated and a series of small amplitude wave was observed. The interfacial wave during the flow tended to be uniform and can be described as two-dimensional wave. As the superficial velocity increases, the 3D wavy flow is observed as depicted in Fig. 10(b). Here, the periodical wave still can be observed. However, the wave perturbation, especially is triggered due to the wave breakup mechanism around the inner wall, often occurs. It causes the presence of irregular wave. Close observation of Fig. 10(b) reveals that small ripple is also found in the 3D wavy flow.

Fig. 10(c) depicts the roll wave phenomena which was found at a higher gas superficial velocity. It is characterized by the presence of the sudden increase of liquid phase acting as rolling wave. It will increase
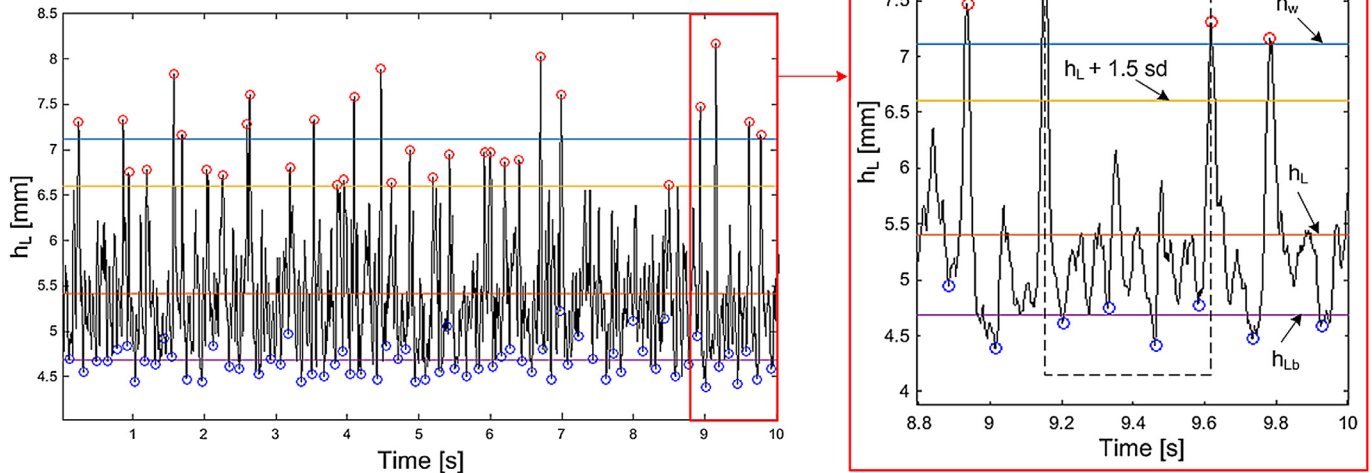
Fig. 9. The example of local film thickness ($J_L = 0.03$ m/s and $J_G = 13$ m/s).

the shear stress along the flows and causes the liquid hold up of the flow decreases. Fig. 10(d) shows the example of entrained droplet and disturbance wave occurred at $J_L = 0.03$ m/s and $J_G = 16$ m/s. The atomization and the droplet deposition around the inner wall is one of the mechanisms leading to the formation of annular flow [7]. At slightly higher liquid flow rate, the presence of hydraulic jump and temporary blockage by liquid film can be observed as shown in Fig. 10(e). This flow pattern is described as pseudo-slug flow as identified by Lin and Hanratty [7]. As found in stratified roll, it is caused by the increase of interfacial shear stress. The liquid phase is able to reach the top of the wall. However, due to the small amount of the liquid, the liquid blockage disappears as the time progressed. Next, the observed flow patterns are plotted and added by transition line as depicted in Fig. 11.

3.2. Interfacial wave parameter

3.2.1. Wave frequency

Fig. 12 shows the effect of J_G and J_L on the wave frequency. From the figure, it is observed that at $J_G < 8$ m/s and in low liquid flow conditions ($J_L < 0.04$ m/s), the wave frequency tends to be higher due to the presence of 2D and 3D wavy flow. In those flow patterns, the periodic and uniform flow still occurs and the large disturbance wave is rarely found. As a result, it produces the higher frequency. However, at $J_G \geq 8$ m/s, the increase of gas superficial velocity on the constant liquid superficial velocity causes an increase in the wave frequency.

There are some previous studies which focus on the wave frequency on the two-phase flow [1,15,35]. However, the proposed correlation related to the wave frequency on the stratified flow has not been discussed yet. The available correlations consider the modified Martinelli Parameter, representing the inertia of the gas and liquid phase, as the main factor affecting the wave frequency [28,29]. Mantilla [29] proposed a correlation to predict the wave frequency on the stratified and annular flow by using nondimensional parameter X and St as shown in Table 1. The X parameter is the Lockhart Martinelli Parameter while St defines the Strauhal Number. They can be described as follows:

$$X = \sqrt{\frac{\rho_L J_L^2}{\rho_G J_G^2}} \tag{3}$$

$$St = \frac{f \cdot D_H}{J_L} \tag{4}$$

where J_L and J_G represent the liquid and gas superficial velocity, ρ_L and ρ_G are liquid and gas density, f describes the wave frequency, and D_H is hydraulic diameter of the pipe.

Bae et al. [28] developed the wave frequency correlation of the stratified flow on the rectangular pipe. However, it was also mentioned that the correlation was only appropriate for the $J_G \geq 15$ m/s. In term of Annular flow, Al Sarkhi et al. [15] have proposed a correlation by using the nondimensional parameter which is developed by Mantila [29] to predict the frequency of the annular flow on the horizontal pipe of 76.2 mm inner diameter.

Fig. 13 depicts the comparison of the present works and the previous studies. Here the horizontal axis is Martinelli Parameter (X) while the Strouhal number (St) is set as the vertical axis. Close observation of the figure reveals that as the Martinelli parameter increases, the Strouhal number decreases. This results indicates that the increase of interaction of interfacial wave is affected by the decrease of Martinelli parameter. Previous studies, such as Mantilla [29], Al Sarkhi et al. [15], and Bae et al. [28], produced the similar trend with the present work. The data of their experimental works as well as the proposed correlation are also plotted in Fig. 13 to elaborate the results more comprehensively. As shown in Fig. 13, It is found that the correlation proposed by Mantila [29] overpredicts the experimental data. While the correlation proposed by Bae et al. [28] overpredicts the experimental data for $X > 0.15$ and underpredicts for $X \leq 0.15$. Next, the correlation of Al Sharki et al. [15] which was built on the basis of experimental data produces a higher value in comparison with the present experimental data as well as the data of Mantila [29] and Bae et al. [28].

The discrepancy shown by previous studies indicates that further analysis should be developed to formulate a better correlation which is able to predict accurately the wave characteristics of the stratified flow. Here, the dimensional analysis was carried out based on the experimental data to reveal the dominant factor affecting the wave frequency. It is generally known that the frequency of the wavy is influenced by numerous factors such as the gas superficial velocity, the liquid superficial velocity, the viscosity of the gas and the liquid, and the density of the gas and liquid. The general function of the wave frequency is written as follows:

$$f = f(Jg, JL, D, \mu L, \mu G, \rho L, \rho g) \tag{5}$$

Furthermore, those variables are summarized in Table 3 which contains the name of the variable, the symbol of the variable, and the

(a) 2D Wave (J_L = 0.03 m/s and J_G = 5 m/s)

(b) 3D Wave (J_L = 0.03 m/s and J_G = 6 m/s)

(c) Roll Wave (J_L = 0.03 m/s and J_G = 8 m/s)

(d) Entrained Droplet and Disturbance Wave (J_L = 0.03 m/s and J_G = 16 m/s)

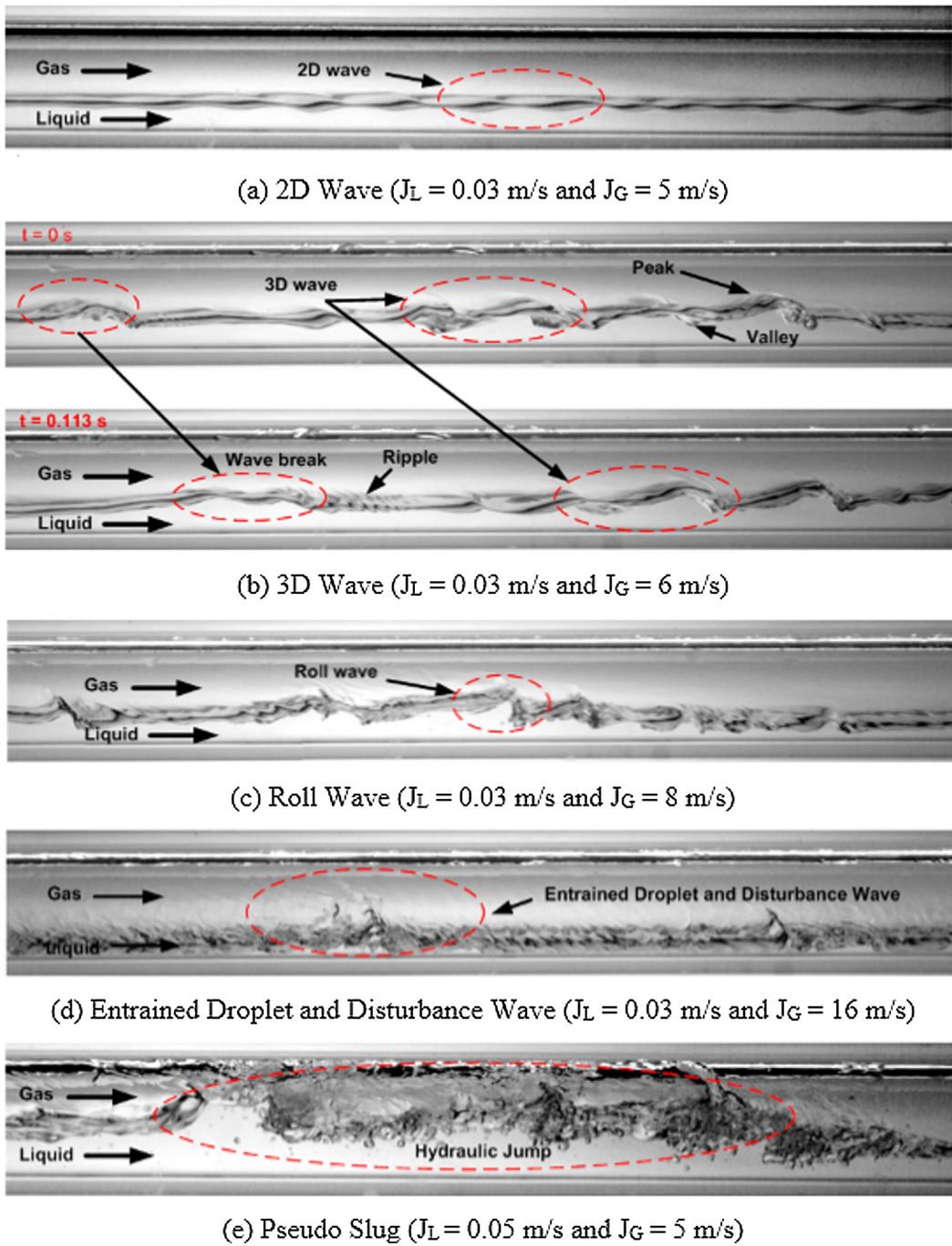(e) Pseudo Slug (J_L = 0.05 m/s and J_G = 5 m/s)

Fig. 10. The example of various wave types.

variable dimension.

From the table by using the pi Buckingham and theory, it is possible to form five Pi dimensionless parameter (Π) by using Pi Buckingham Theorem. In the present work, The D, J_L, and ρ_L were chosen as a repeated variable. Those can be written as follows:

$$\prod_1 = \frac{f \cdot D}{J_L} \tag{6}$$

$$\prod_2 = \frac{J_G}{J_L} \tag{7}$$

$$\prod_3 = \frac{\rho_G}{\rho_L} \tag{8}$$

$$\prod_4 = \frac{\mu_L}{J_L \rho_L D} \tag{9}$$

$$\prod_5 = \frac{\mu_G}{J_L \rho_L D} \tag{10}$$

It is then processed to form a simpler non dimensional parameter. Here, Π_6 and Π_7 were utilized to simplify the available parameter. The mathematical operation process is described as follows:

$$\prod_6 = \frac{\Pi_2 \cdot \Pi_3}{\Pi_5} = \frac{\left[\frac{J_G}{J_L}\right] \cdot \left[\frac{\rho_G}{\rho_L}\right]}{\left[\frac{\mu_G}{J_L \rho_L D}\right]} = \frac{J_G \rho_G D}{\mu_G} \tag{11}$$
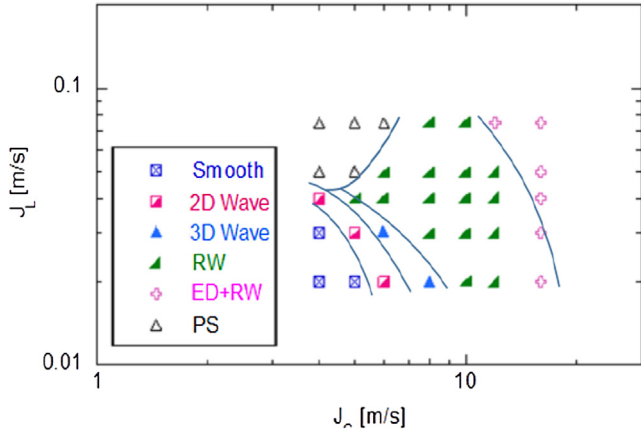
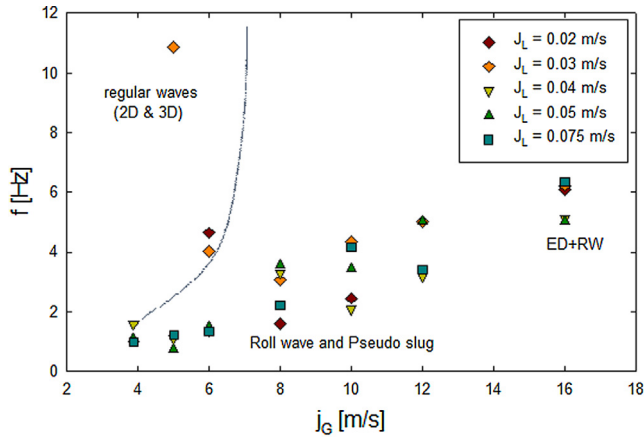**Fig. 11.** The wave regime map for the present study.

Fig. 12. The effect of J_G and J_L on the variation to wave frequency.
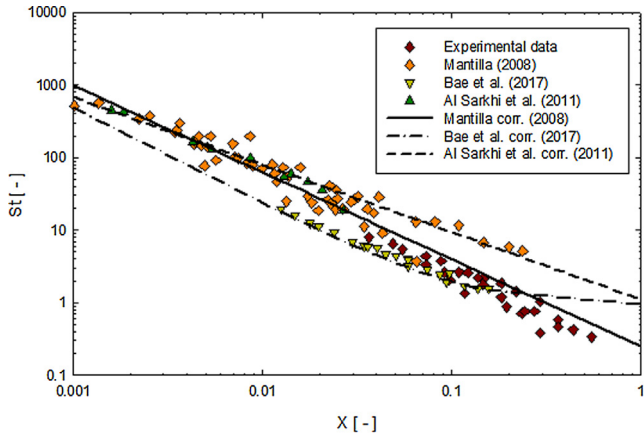

Fig. 13. The comparison of the result of the present work with the previous studies.

$$\prod_7 = \sqrt{\prod_2 \cdot \prod_3^2} = \sqrt{\frac{\rho_G}{\rho_L} \cdot \left(\frac{J_G}{J_L}\right)^2} \tag{12}$$

As a result, the general form of the function which contains all of the dimensionless parameters can be expressed as follows:

$$\prod_1 = f\left(\prod_4, \prod_6, \prod_7\right) \tag{13}$$

Table 3
The dimension of the variable.

The variable	Symbol	The variable dimension		
		M	L	T
The frequency of wave	f			−1
The diameter of the pipe	D		1	
The superficial velocity of the liquid	J_L		1	−1
The superficial velocity of gas	J_G		1	−1
The dynamic viscosity of the liquid	μ_L	1	−1	−1
The dynamic viscosity of the gas	μ_G	1	−1	−1
The density of the liquid	ρ_L	1	−3	
The density of the gas	ρ_g	1	−3	

$$\frac{f \cdot D}{J_L} = a\left[\frac{\mu_L}{J_L \rho_L D} x \frac{J_G \rho_G D}{\mu_G}\right]^b \left[\sqrt{\frac{\rho_G}{\rho_L} \cdot \left(\frac{J_G}{J_L}\right)^2}\right]^c \tag{14}$$

where *a*, *b*, and *c* represent the fitting coefficient of the formula. Next, the Strouhal Number (S_t), the liquid Reynolds number (Re_L), the gas Reynolds number (Re_G), and the Martinelli parameter (X) are generally formulated as follows:

$$\frac{f \cdot D}{J_L} = S_t \quad S_t = \text{Strouhal Number} \tag{15}$$

$$\frac{J_L \rho_L D}{\mu_L} = Re_L \quad Re_L = \text{liquid Reynolds number} \tag{16}$$

$$\frac{J_G \rho_G D}{\mu_G} = Re_G \quad Re_G = \text{gas Reynolds number} \tag{17}$$

$$\sqrt{\frac{\rho_G}{\rho_L} \cdot \left(\frac{J_G}{J_L}\right)^2} = \frac{1}{X} \quad \text{X= Martinelli parameter} \tag{18}$$

Next, the Eqs. (15)–(18) are substituted into the Eq. (14), and the result is written as follows:

$$St = a\left[\frac{Re_G}{Re_L}\right]^b \left[\frac{1}{X}\right]^c \tag{19}$$

To determine the fitting coefficient of Eq. (19), the fitting process is carried out by using the present experimental data which is focused on the irregular waves flow pattern (roll-wave, pseudo-slug, and the entrained droplet + roll wave). Moreover, the data of previous studies [14,28] were also utilized to produce well-represented correlation. The final form of wave frequency correlation is written as follows.

$$St = 0.215\left[\frac{Re_G}{Re_L}\right]^{0.08} X^{-0.912} \tag{20}$$

The proposed correlation should be evaluated to compare the result of the predicted wave frequency with that of obtained by image processing technique. Fig. 14 shows the comparison of the result of proposed correlation and the experimental data. It is observed that in general, the proposed correlation shows a good agreement with the measured data. Most of the data lie under 50% error. In addition, the further analysis is carried out to clarify the error value. The Mean Absolute Percentage Error (MAPE) is formulated as follows:

$$MAPE = \frac{1}{n}\sum_{i=1}^{n}\left|\frac{X_{pred,i} - X_{\exp,i}}{X_{\exp,i}}\right| \times 100\% \tag{21}$$

where $X_{pred,i}$ is the Strouhal number obtained from the proposed correlation, $X_{\exp,i}$ is the data obtained from the experiment, and n defines the number of data. Based on the analysis of the data obtained by image processing technique, the calculated MAPE is 23.0%. Therefore, it can be concluded that the proposed formula can accurately predict the frequency of the wave represented by the Strouhal number. While the MAPE of the data of the Bae et al. [28], and Shi and
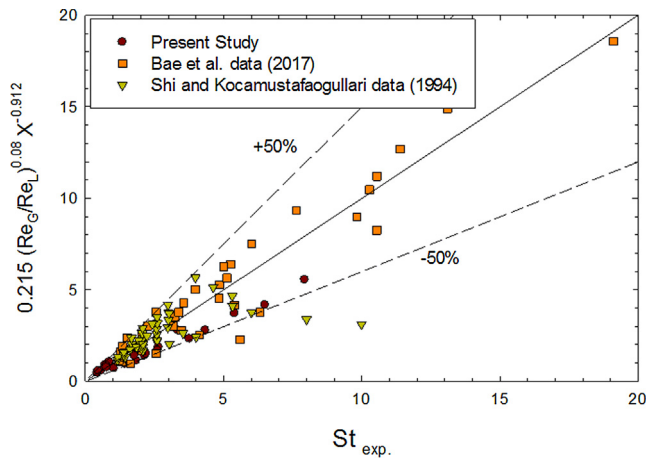
Fig. 14. The performance of new correlation for wave frequency.

Fig. 16. The comparison of the experimental data with previous studies.

Kocamustafaogullari [14] are, 21.8% and 23.9%, respectively. To conclude, the Eq. (20) can be interpreted the phenomena of wave frequency as follows.

– The ratio between Reynolds Number of the gas and liquid plays an important role in the wave frequency. As the ratio of Reynolds number increases, the Stouhal number, representing the wave frequency ratio, increases. It shows the similar tendency with the investigation conducted by Ousaka et al. [35]. The Reynolds number can be defined as the ratio of inertia force and viscous force. Therefore, the viscosity of the fluid also influences the wave frequency. As concluded by Setyawan et al. [1], the increase of liquid viscosity causes the frequency of the wave decreases.
– The increase of the Martinelli Parameter leads the decrease of the Strouhal number. The Martinelli Parameter is defined as the ratio between the liquid Froude number and the gas Froude number. Meanwhile, the Froude number, which is described as the ratio between the inertia force and the gravitational effect, is strongly affected by the phase velocity. The results also confirm to that of the Setyawan et al. [1] who reported that the increase of the gas and liquid superficial velocity also increases the wave frequency.

3.2.2. Wave velocity

Fig. 15 depicts the effect of J_G and J_L on the wave velocity. The increase of the J_L under the constant J_G causes the wave velocity increases except for the pseudo slug phenomena. At low J_G and high J_L, each individual wave has different propagation velocity. It significantly increases the possibility of wave coalescence during the flow. Due to the small amount of the water, the pseudo slug pattern is formed. It is
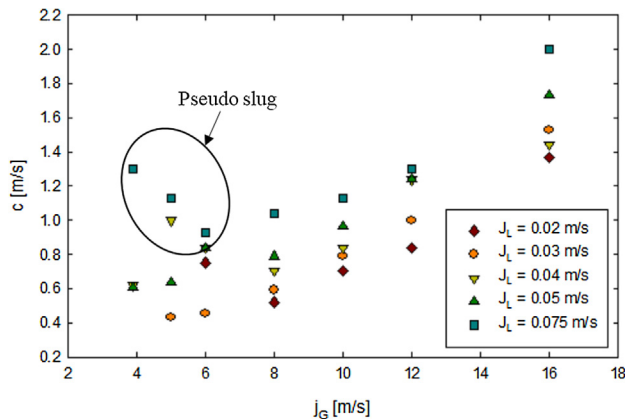

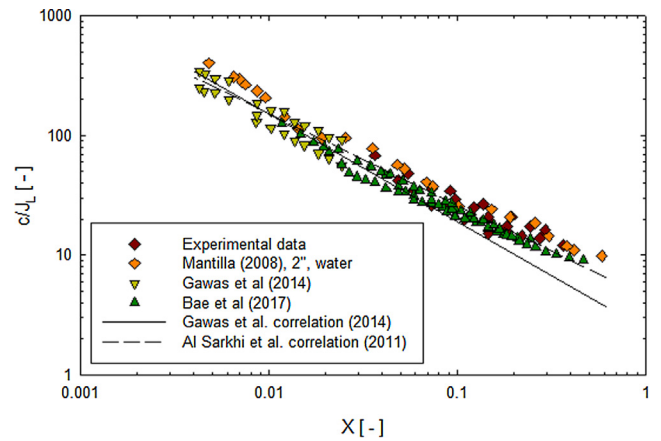**Fig. 15.** The effect of J_G and J_L on the wave velocity.

characterized by the presence of a series of bigger wave which temporarily blocks the cross-sectional area of the pipe. As the J_G increases, the wave breakup events is more dominant in comparison to the wave coalescence so both of the frequency and the velocity of the wave becomes stable.

The comparison of the present work with the previous studies is depicted in Fig. 16 where the Martinelli parameter and the ratio of wave velocity with liquid superficial velocity are chosen as X and Y axis, respectively. In general, a similar result between the present and previous works is found. However, it is noted that the correlation proposed by Al Sarkhi et al. [15] underpredicts the present experimental data. It is mainly due to the different experimental condition. The correlation of the Al Sarkhi et al. [15] was arranged by using the experimental data on the high gas superficial velocity. While in comparison the result of Gawas et al. [17], the data tends to show good agreement.

To obtain the correlation of the wave velocity, dimensional analysis, as implemented in the previous section, was conducted. It is followed by fitting process present experimental data as well as the data gathered from previous literatures [14,28,29], especially where the $J_G \geq 5$ m/s. By considering the important parameter affecting the wave velocity, the correlation to predict the wave velocity is written as follows:

$$c/J_L = 4.786\left[\frac{Re_G}{Re_L}\right]^{0.18} X^{-0.51} \tag{22}$$

From the Eq. (22), it is found that ratio of gas and liquid Reynolds number shows the positive effect to the ratio of wave velocity and the liquid superficial velocity. As the ratio of the gas and liquid Reynolds number increases, the ratio of wave velocity and the liquid superficial velocity increases too. It shows the similar tendency with the investigation conducted by Ousaka et al. [35]. Meanwhile, Martinelli parameter which represents the ratio between the liquid Froude number and the gas Froude number shows the negative effect on the Strouhal number. It shows the similar tendency with the investigation conducted by Gawas et al. [17].

The comparison of the proposed correlation with the present experimental data is shown in Fig. 17. In general, the predicted value shows a good agreement with the experimental data of present study. The MAPE is around 13.8%. Furthermore, the result of previous studies [14,28,29] was also used to develop correlation. Next, the available data was also analyzed to obtain the error value of proposed correlation. The MAPE between the predicted value and the actual data of Mantilla [29], Bae et al. [28], and Shi and Kocamustafaogullari [14] were 15.3%, 14.1%, 40.3% and 9.5%, respectively.

3.2.3. Wave amplitude
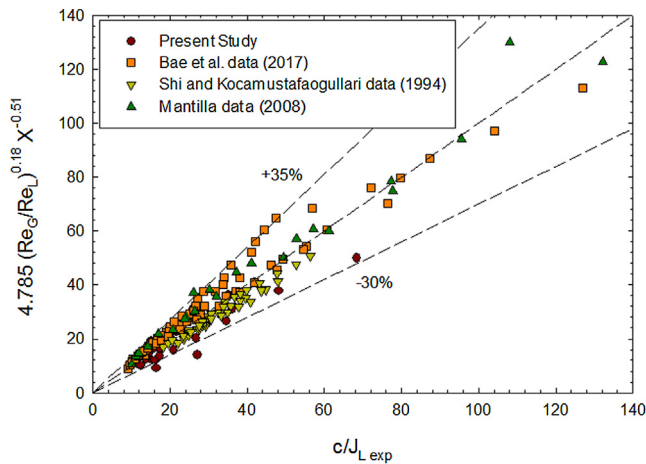
The effect of J_G and J_L on the wave amplitude (Δh_w) is clearly

Fig. 17. The comparison of the proposed wave velocity correlation with the experimental data.
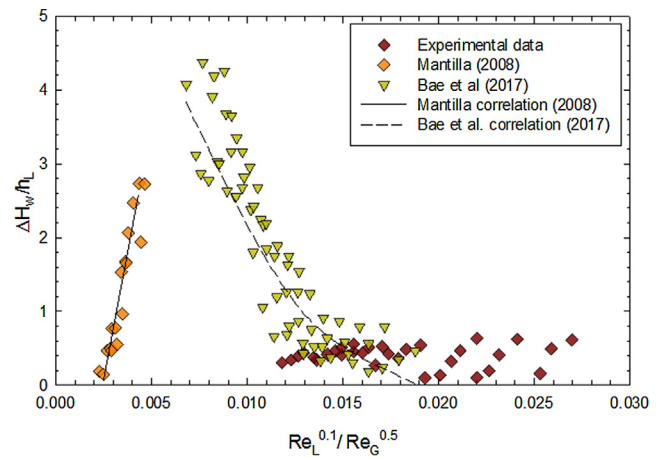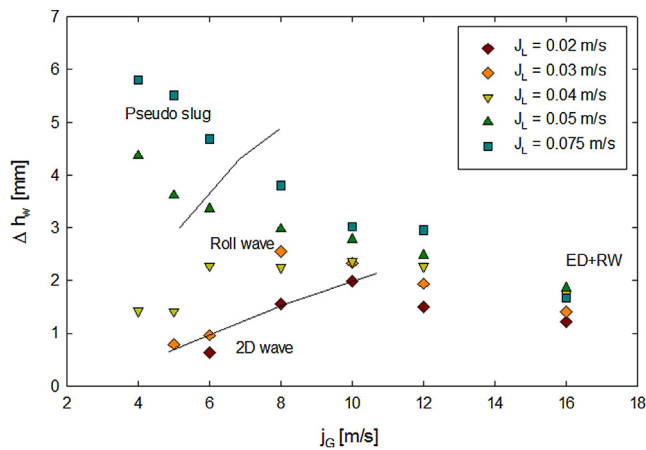

Fig. 18. The effect of J_G and J_L on the Δh_w.

presented in Fig. 18. Under the constant J_G, the Δh_w tends to be higher as the J_L increases. On the other hand, the effect of J_G seems to be more complex since it also depends on the J_L. At the $J_L \geq 0.04$ m/s, the increase of the J_G causes the Δh_w decreases. It is due to the competition between the wave break up and the wave coalescence. As the J_G increases, the wave breakup overcomes the wave coalescence to produce a lower wave amplitude. At the $J_L < 0.04$ m/s, the Δh_w also increases as the increase of the J_G because of the regime transition between 2D and 3D wave into the roll wave. Then it tends to decrease as the flow pattern change from the roll wave flow into the roll wave + entrained droplet.

The ratio of the Reynolds number ($Re_L^{0.1}/Re_G^{0.5}$) is considered as the only dominant factor affecting the wave amplitude as concluded by Mantilla [29] and Bae et al. [28]. The comparison of the experimental data with the proposed correlation of the Mantilla [29] and Bae et al. [28] is shown in Fig. 19. From the figure, it is found that in comparison to present experimental data, the correlation of Mantila [29] is far predicted rather than the experimental data. Meanwhile, the correlation of the Bae et al. [28] shows that at the ($Re_L^{0.1}/Re_G^{0.5}$) < 0.015, the value tends to be overpredicted while at the ($Re_L^{0.1}/Re_G^{0.5}$) ≥ 0.015, it is observed that the value is underpredicted. In summary, both of proposed correlation can't predict the phenomena of the wave amplitude on the present experimental studies.

Therefore, the present study also propose a new correlation of the wave amplitude on the basis of the various important parameter. Next, the dimensional analysis on the present experimental data where the $J_G > 6$ m/s as well as the data of Bae et al. [28] was conducted to

produce the correlation of the wave amplitude written as follows.

$$\frac{\Delta h_w}{h_L} = 0.03 \left[\frac{Re_G}{Re_L} \right]^{6.0} X^{5.7} \tag{23}$$

As shown in Eq. (23), the ratio of gas and liquid Reynolds number and Martinelli Parameter show positive effect on the ratio of the wave amplitude and the film thickness. As the Reynolds number increases, the ratio of the wave amplitude and the film thickness also increases. The Martinelli Parameter, which is the function of the gas and liquid mass flow rate, plays an important role in the wave formation of the two-phase flow.

The proposed correlation was compared to the experimental data as shown in Fig. 20. The data of the Bae et al. [28] was also added to the figure. Close observation of Fig. 20 reveals that the proposed correlation predicts the ratio of the wave amplitude and the film thickness well. The MAPE between predicted and actual value of the data of the present study and Bae et al. [28] were 22.54% and 21.57%, respectively.

3.2.4. The wavelength

Fig. 21 depicts the effect of J_G and J_L on the wavelength. It is noted that the liquid superficial velocity plays an important role in the wavelength characteristic. At $J_L \geq 0.05$ m/s, the increase of the J_G, in general, leads the decrease of the L_w. The pseudo slug, which dominantly occurs at low J_G and high J_L ($J_G \leq 6$ m/s and JL ≥ 0.05 m/s), is characterized by the presence of high wave velocity which flows in low

Fig. 19. The comparison of the experimental data of the wave amplitude with the previous studies.

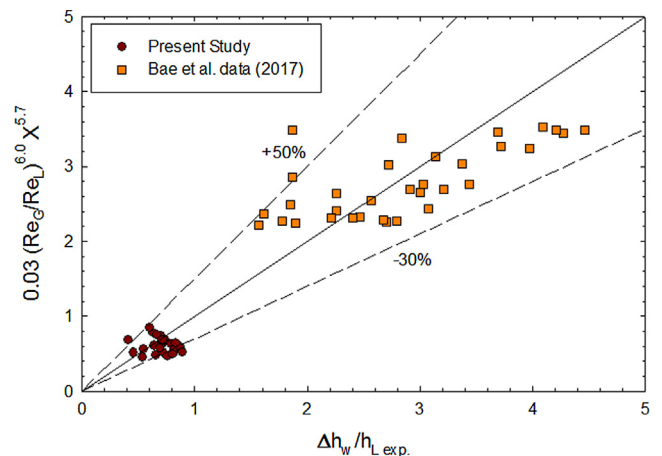**Fig. 20.** The comparison of the proposed wave amplitude correlation with the experimental data.
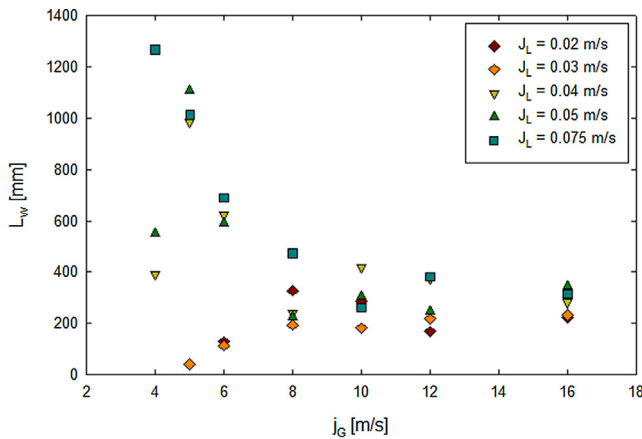
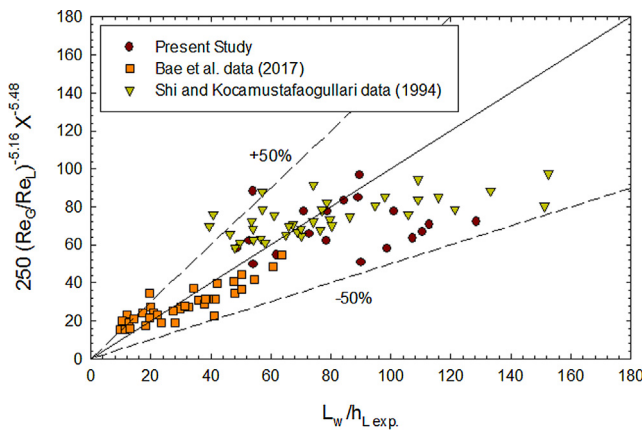**Fig. 21.** The effect of J_G and J_L on the L_w.

Fig. 22. The comparison of the proposed wave length correlation with the experimental.

frequency to produce long wavelength. As the increase of J_G, the difference between gas and liquid inertia also becomes higher leading the wave breakup occurs more frequently. As a result, the wavelength increases. Whereas in the low liquid loading condition ($J_L < 0.05$ m/s), the increase of J_G tends to increase the L_W. It is due to the occurrence of regime transition form periodic wave, which contains a series of small waves, to the disturbance wave. One of the main characteristics of disturbance wave is the presence of high amplitude wave during the flow.

The dimensional analysis is also used to reveal the dominant factor affecting the L_w. The fitting process was done by using the present experimental data on the $J_G > 6$ m/s. Furthermore, the data of Shi and Kocamustafaogullari [14] and Bae et al. [28] were also used to determine the fitting coefficient. Finally, the correlation of the wavelength is obtained. It is written as follows:

$$\frac{L_w}{h_L} = 250 \left[\frac{Re_G}{Re_L} \right]^{-5.07} X^{-5.48}$$

(24)

On the contrary of the proposed correlation of the wave amplitude, it is observed that the ratio of gas and liquid Reynolds number and Martinelli parameter shows the negative effect of the ration of the wavelength and the average film thickness. The increases of the gas and liquid Reynolds number, as well as the Martinelli parameter, decreases the ratio of-of the ration of the wavelength and the average film thickness. Next, Fig. 22 shows the comparison of the proposed correlation and the experimental result. It is important to be noted that the available correlation of the wavelength has not been found yet. So the presence of this correlation is important. As shown in the figure, the

MAPE between the predicted value and the experimental data of the present study, Bae et al. [28] and Shi and Kocamustafaogullari [14] were 23.4%, 22.0% and 22.4%, respectively.

4. Conclusion

In the present work, the image processing technique was applied to determine the essential parameter on the wave dynamic characteristics of the stratified flow. The result was analyzed to reveal the effect of the change of gas and liquid superficial velocity on each parameter. In addition, several correlations were proposed by using the dimensional analysis. The results are summarized as follows:

a. The ratio of Reynolds number and Martinelli parameter plays an important role in the proposed correlation of the wave frequency, wave velocity, wave amplitude, and the wave amplitude.
b. On the proposed correlation of the wave frequency, the ratio of Reynolds number shows the positive effect on the Strouhal number. On the other hand, the increase of the Martinelli parameter shows the negative effect on the Strouhal number. Here, it is found that The Mean Absolute Percentage Error of the proposed correlation is 23.0%.
c. The proposed correlation of the wave velocity shows that the increase of the ratio of the gas and liquid Reynolds number increase the ratio of the wave velocity and the liquid superficial velocity. On the other hand, the increase of the Martinelli parameter shows the negative effect on the ratio of the wave velocity and the liquid superficial velocity. The Mean Absolute Percentage Error of the proposed correlation of the wave velocity is 13.8%.
d. The proposed correlation of the wave amplitude reveals that the increase of the ratio of the gas and liquid Reynolds number and the Martinelli parameter also increase the ratio of the wave amplitude and the average film thickness. The Mean Absolute Percentage Error of the proposed correlation of the wave amplitude is 22.54%.
e. On the contrary of the proposed correlation of the wave amplitude, the dimensional analysis of the wavelength shows that the ratio of the gas and liquid Reynolds number and the Martinelli parameter also have the negative effect on the ratio of the wave amplitude and the average film thickness. The proposed correlation shows a satisfying performance with The Mean Absolute Percentage Error of the proposed correlation is 23.4%.

Conflict of interest

The authors declared that there is no conflict of interest.

References

[1] A. Setyawan, Indarto, Deendarlianto, the effect of the fluid properties on the wave velocity and wave frequency of gas–liquid annular two-phase flow in a horizontal pipe, Exp. Therm. Fluid Sci. J. 71 (2016) 25–41.
[2] C. Tsotzi, N. Andritsos, Interfacial shear stress in wavy gas-lquid flow in horizontal pipes, Int. J. Multiphase Flow 54 (2013) 43–54.
[3] Y. Taitel, A.E. Dukler, A model for predicting flow regime transitions in horizontal and near horizontal gas-liquid flow, AIChE J. 22 (1976) 47–55.
[4] P.Y. Lin, T.J. Hanratty, Prediction of the initiation of slugs with linear stability theory, Int. J. Multiphase Flow 12 (1986) 79–98.
[5] M. Otten, K. Klinkspoor, H.C.J. Hoefsloot, P.J. Hamersma, Wave characteristics during concurrent gas-liquid pipe flow, Exp. Therm. Fluid Sci. J. 19 (1999) 140–150.
[6] O. Dinaryanto, Y.A.K. Prayitno, A.I. Majid, A.Z. Hudaya, Y.A. Nusirwan, A. Widyaparaga, Indarto, Deendarlianto, experimental investigation on the initiation and flow development of gas-liquid slug two-phase flow in a horizontal pipe, Exp. Therm. Fluid Sci. J. 81 (2017) 93–108.
[7] P.Y. Lin, T.J. Hanratty, Effect of pipe diameter on flow patterns for air-water flow in horizontal, Int. J. Multiphase Flow 13 (4) (1987) 549–563.
[8] D.E. Woodmansee, T.J. Hanratty, Mechanism for the removal of droplets from a liquid surface by a parallel air how, Chem. Eng. Sci. 24 (1969) 299.
[9] A.Z. Hudaya, H.Y. Kuntoro, O. Dinaryanto, Indarto and Deendarlianto, experimental investigation on the interfacial characteristics of stratified air-water two-phase flow in a horizontal pipe, AIP Conference Proceedings, 2016, p. 040012.

[10] P.L. Spedding, V.T. Nguyen, Regime map for air water two-phase flow, Chem. Eng. Sci. 35 (1979) 779–793.

[11] X.T. Chen, X.D. Cai, J.P. Brill, Gas liquid stratified-wavy flow in horizontal pipe-lines, ASME J. Energy Res. Tech. 119 (4) (1997) 209–216.

[12] M. Fernandino, T. Ytrehus, Determination of flow sub-regimes in stratified air––water channel flow using LDV spectra, Int. J. Multiphase Flow 32 (2006) 436–446.

[13] H.C. Kang, M.H. Kim, Measurement of three-dimensional wave form and interfacial area in an air water stratified flow, Nucl. Eng. Des. (1992) 347–360.

[14] J. Shi, G. Kocamustafaogullari, Interfacial meusurements in horizontal stratified flow pattern, Nucl. Eng. Des. (1994) 81–96.

[15] A. Al-Sarkhi, C. Sarica, K. Magrini, Inclination effects on wave characteristics in annular gas–liquid flows, AIChE J. 58 (4) (2011) 1018–1029.

[16] W. Meng, Low Liquid Loading Gas-Liquid Two-Phase Flow in Near Horizontal Pipes. PhD. Dissertation, The University of Tulsa, 1999.

[17] K. Gawas, H. Karami, E. Pereyra, A. Al-sarkhi, C. Sarica, Wave characteristics in gas–oil two phase flow and large pipe diameter, Int J. Multiphase Flow 63 (2014) 93–104.

[18] M. Birvalski, M.J. Tummers, R. Delfos, R. Henkes, Laminar-turbulent transition and wave-turbulence interaction in stratified horizontal two–phase pipe flow, J. Fluid Mech. 780 (2015) 439–456.

[19] A. Ayati, J. Kolaas, A. Jensen, G. Johnson, A PIV investigation of stratified gasliquid flow in a horizontal pipe, Int J. Multiphase Flow 61 (2014) 129–143.

[20] G.A. Montoya, Deendarlianto, D. Lucas, Image processing based study of interfacial behavior of the countercurrent gas-liquid two-phase flow in hot leg of a PWR, Sci. Technol. Nucl. Install. (2012).

[21] M.S. Castro, O.M.H. Rodriguez, Interfacial waves in stratified viscous oil–water flow, Exp. Therm. Fluid Sci. J. 62 (2015) 65–98.

[22] H.Y. Kuntoro, A.Z. Hudaya, O. Dinaryanto, A.I. Majid, Deendarlianto An improved algorithm of image processing technique for film thickness measurement in a horizontal stratified gas-liquid two-phase flow, AIP Conference Proceedings, 2016, p. 040010.

[23] R.E.M. Morales, M.J. da Silva, E.N. Santos, L. Dorini, C.E.F. do Amaral, Images analysis of horizontal two-phase slug flows, Proceedings of the ASME International Mechanical Engineering Congress & Exposition Volume 6: Fluids and Thermal

[24] C.E.F. do Amaral, R.F. Alves, M.J. da Silva, L.V.R. Arruda, L. Dorini, R.E.M. Morales, D.R. Pipa, Image processing techniques for high-speed videometry in horizontal two-phase slug flows, Flow Meas. Instrum. 33 (2013) 257–264.

[25] A. Widyatama, O. Dinaryanto, Indarto, deendarlianto, the development of image processing technique to study the interfacial behavior of air-water slug two-phase flow in horizontal pipes, Flow Meas. Instrum. 59 (2018) 168–180.

[26] S.V. Paras, A.J. Karabelas, Properties of the liquid layer in horizontal annular flow, Int. J. Multiphase Flow 7 (4) (1991) 439–454.

[27] I. Mantilla, Mechanistic Modeling of Liquid Entrainment in Gas in Horizontal Pipes, PhD Dissertation, U. of Tulsa OK, 2008.

[28] Deendarlianto, A. Ousaka, T. Kariyasaki, Fukano, investigation of liquid film be-havior at the onset of flooding during adiabatic counter-current air–water two-phase flow in an inclined pipe, Nucl. Eng. Des. 235 (2005) 2281–2294.

[29] B. Bae, T. Ahn, J. Jeong, K. Kim, B. Yun, Characteristics of an interfacial wave in a horizontal air-water stratified flow, Int. J. Multiphase Flow 97 (2017) 197–205.

[30] R. Kong, A. Rau, C. Lu, S. Kim, S. Bajorek, K. Tien, C. Hoxie, Experimental study of interfacial structure of horizontal air-water two-phase flow in a 101.6 mm ID pipe, Exp. Therm. Fluid Sci. 93 (2018) 93–108.

[31] N. Andritsos, Statistical analysis of waves in horizontal stratified gas–liquid flow, Int. J. Multiphase Flow, Vo. 18 (1992) 465–473.

[32] Deendarlianto, A. Moeso, O. Widyaparaga, Dinaryanto, khasani, indarto, CFD stu-dies on the gas-liquid plug two-phase flow in a horizontal pipe, J. Petrol. Sci. Eng. 147 (2016) 779–787.

[33] C. Vallee, T. Nariai, T. Futatsugi, A. Tomiyama, D. Lucas, M. Murase, Experimental characterisation of the interfacial structure during counter-current flow limitation in a model of the hot leg of a PWR, Sci. Technol. Nucl. Install. (2012).

[34] B.G. Gowri, V. Hariharan, S. Thara, V. Sowmya, S.S. Kumar, K.P. Soman, 2D Image data approximation using Savitzky Golay filter-Smoothing and differencing, Int. Multi-Conf. IEEE (2013) 365–371.

[35] A. Ousaka, I. Morioka, T. Fukano, Air-water annular two-phase flow in horizontal and near horizontal tubes: disturbance wave characteristics and liquid transporta-tion, Jpn. J. Multiphase Flow 6 (9) (1992) 80–87.